Eddy-Current-Effect Homogenization of Windings in Harmonic-Balance Finite Element Models

Ruth V. Sabariego[1] and Johan Gyselinck[2]
[1] KU Leuven, Dept. Electrical Engineering, Campus EnergyVille, Belgium
[2] Université Libre de Bruxelles (ULB), BEAMS Dept., Belgium

The eddy-current effects in windings, i.e. skin and proximity effects, can be macroscopically modelled via a complex frequency-dependent impedance and reluctivity. In this work, these two complex quantities are further embedded in a harmonic-balance finite element model for arriving at the steady-state solution. The proposed approach is validated through a 2D model of an inductor with pulse-width modulated voltage supply. Both local and global quantities are shown to agree well with brute-force simulation results. The computational cost of both approaches is compared.

***Index Terms*—Eddy currents, finite element methods, harmonic balance, proximity effect, skin effect.**

I. Introduction

THE accurate consideration of skin and proximity effects in the winding of high-frequency electromagnetic devices through the fine discretization of each turn is most often unworkable in practice. Frequency-domain homogenization techniques provide a closed-form continuous representation of the homogenized winding, see e.g. [1], [2] and references herein. Proximity and skin effects are considered by a complex reluctivity in the homogenized winding window and a complex impedance in the electrical circuit equations, respectively. A general approach to identify these frequency-dependent parameters is proposed in [3], along with a time-domain extension and three-dimensional application in [4].

In this paper, we aim at embedding this winding homogenization technique in a harmonic-balance (HB) computation for arriving at a periodic steady-state solution, whereby local and global variables (flux density, currents, ...) are approximated by a truncated Fourier series; this approach may be an interesting alternative to plain time-stepping, particularly when the transient is long [5]. By extending the set of considered frequencies, starting from the fundamental one f_1 (period $T_1 = 1/f_1$), one can compromise between accuracy and computational cost.

Several HB approaches have been proposed, e.g. [6], [7], which are more or less efficient and/or arduous to implement. A thorough mathematical analysis with error estimators can be found in [8]. We embrace the Galerkin time-domain variant presented in [9], as it allows to straightforwardly include magnetic saturation, nonlinear lumped components in the electrical circuit (e.g. diodes), and especially rotation [10].

The proposed multi-frequency approach, i.e. with winding homogenization, is validated by means of an axisymmetric model of an inductor.

II. Generic Field-Circuit ODEs

We consider a generic 2D eddy-current problem with so-called stranded and massive conductors (subscripts S and M, resp.) and its magnetic vector potential $\boldsymbol{a}$ formulation; the extension to other formulations is straightforward. The first-order ordinary differential equations (ODEs) arising from its FE discretization (with n_w shape and test functions) in terms of the unknowns column vector $\mathbf{A} = \left[a_1(t) \cdots a_{n_\mathrm{w}}(t)\right]^\top$ features the reluctivity-dependent stiffness matrix $\mathbf{S}(\nu)$, the conductivity-dependent eddy-current matrix $\mathbf{T}_M(\sigma)$, and right handside column vectors accounting for the sources, i.e. the current in the stranded conductors (uniform current density) and the voltage across the massive conductors (non-uniform current density due to skin and proximity effects):

$$\mathbf{S}\,\mathbf{A} + \mathbf{T}_M \frac{\mathrm{d}\mathbf{A}}{\mathrm{d}t} = \mathbf{K}_M^\top \mathbf{R}_M^{-1} \mathbf{V}_M + \mathbf{K}_S^\top \mathbf{I}_S \,, \tag{1}$$

$$\mathbf{V}_M = \mathbf{R}_M \mathbf{I}_M + \mathbf{K}_M \frac{\mathrm{d}\mathbf{A}}{\mathrm{d}t} \,, \tag{2}$$

$$\mathbf{V}_S = \mathbf{R}_S \mathbf{I}_S + \mathbf{K}_S \frac{\mathrm{d}\mathbf{A}}{\mathrm{d}t} \,, \tag{3}$$

where $\mathbf{I}_S(t)$, $\mathbf{I}_M(t)$, $\mathbf{V}_S(t)$ and $\mathbf{V}_M(t)$ comprise n_S or n_M currents and voltages; diagonal matrices $\mathbf{R}_M$ and $\mathbf{R}_S$ comprise the respective resistances (DC value for the massive conductors); $\mathbf{K}_M$ ($n_\mathrm{M} \times n_\mathrm{w}$) and $\mathbf{K}_S$ ($n_\mathrm{S} \times n_\mathrm{w}$) are connectivity matrices.

Electrical circuit coupling can be considered via n_l independent loops and linked loop-current column vector $\mathbf{I}_l(t)$:

$$\mathbf{D}_{Sl}^\top \mathbf{V}_S + \mathbf{D}_{Ml}^\top \mathbf{V}_M + \mathbf{R}_l \mathbf{I}_l + \mathbf{L}_l \frac{\mathrm{d}\mathbf{I}_l}{\mathrm{d}t} = \mathbf{V}_l \,, \tag{4}$$

where $\mathbf{D}_{Sl}$ ($n_\mathrm{S} \times n_l$) and $\mathbf{D}_{Ml}$ ($n_\mathrm{M} \times n_l$) are connectivity matrices (with 0, 1 and -1 elements, with $\mathbf{I}_S = \mathbf{D}_{Sl}\mathbf{I}_l$ and $\mathbf{I}_M = \mathbf{D}_{Ml}\mathbf{I}_l$), and with the inclusion of a number of lumped resistances, inductances and voltage sources via square loop matrices $\mathbf{R}_l$ and $\mathbf{L}_l$, and righthand side term $\mathbf{V}_l(t)$. Current sources and capacitances can also be considered. Alternatively, the nodal method can be adopted [11]. Any nonlinearity in the FE model and circuit is ignored for sake of simplicity.

Equations (1)-(4) can be written in a block matrix form as:

$$\mathbf{M}\,\mathbf{X}(t) + \mathbf{N}\,\frac{\mathrm{d}\mathbf{X}}{\mathrm{d}t} = \mathbf{F}(t) \,, \tag{5}$$

$$\mathbf{X}(t) = \left[\, \mathbf{A} \;\; \mathbf{V}_M \;\; \mathbf{I}_l \,\right]^\top \,, \quad \mathbf{F}(t) = \left[\, \mathbf{0} \;\; \mathbf{0} \;\; \mathbf{V}_l \,\right]^\top \,, \tag{6}$$

Manuscript received November 20, 2016. Corresponding author: R. V. Sabariego (email: ruth.sabariego@kuleuven.be)

$$\mathbf{M}=\begin{bmatrix}\mathbf{S} & -\mathbf{K}_M^\top\mathbf{R}_M^{-1} & -\mathbf{K}_S^\top\mathbf{D}_{Sl}\\ \mathbf{0} & \mathbb{1} & -\mathbf{R}_M\mathbf{D}_{Ml}\\ \mathbf{0} & \mathbf{D}_{Ml}^\top & \mathbf{R}_l+\mathbf{R}_{Sl}\end{bmatrix},\quad \mathbf{N}=\begin{bmatrix}\mathbf{T}_M & \mathbf{0} & \mathbf{0}\\ -\mathbf{K}_M & \mathbf{0} & \mathbf{0}\\ \mathbf{D}_{Sl}^\top\mathbf{K}_S & \mathbf{0} & \mathbf{L}_l\end{bmatrix}, \tag{7}$$

with $\mathbf{R}_{Sl}=\mathbf{D}_{Sl}^\top\mathbf{R}_S\mathbf{D}_{Sl}$ ($n_l\times n_l$) and $\mathbb{1}$ the identity matrix.

The brute-force skin- and proximity-effect modelling of a coil consist in considering each turn as a massive conductor (e.g. $n_\mathrm{M}=120$ as in section V) and the series connection of all turns via the circuit equations. Instead, the homogenized winding is modelled as one stranded conductor ($n_\mathrm{S}=1$ and $n_\mathrm{M}=0$), as further developed in section IV.

III. Harmonic-Balance Approach

Each of the $n=n_\mathrm{w}+n_\mathrm{M}+n_l$ unknowns in $\mathbf{X}(t)$ can be expressed as a truncated Fourier series considering n_f frequencies f_k, $k=1,2,\ldots$, integer multiples of fundamental frequency f_1 (period $T_1=1/f_1$), or angular frequencies $\omega_k=2\pi f_k$, for a total of $n_\mathrm{h}=2n_\mathrm{f}$ harmonic (cosine or sine) basis functions (BFs), and $n\cdot n_\mathrm{h}$ unknown coefficients collected in column vectors $\boldsymbol{\mathcal{H}}(t)$ and $\mathbf{X}^\mathrm{H}$ respectively:

$$\boldsymbol{\mathcal{H}}(t)=\begin{bmatrix}h_1\cdots h_{n_\mathrm{h}}\end{bmatrix}^\top=\begin{bmatrix}\cdots & \cos(\omega_k t) & \sin(\omega_k t) & \cdots\end{bmatrix}^\top, \tag{8}$$

$$\mathbf{X}(t)=\left(\mathbb{1}\otimes\boldsymbol{\mathcal{H}}(t)^\top\right)\mathbf{X}^\mathrm{H}, \tag{9}$$

where $\otimes$ denotes the Kronecker product. For the sake of simplicity, a DC term (with unitary BF) is not considered [9].

These n_h cosine and sine BFs are mutually orthogonal:

$$\frac{2}{T_1}\int_0^{T_1}\boldsymbol{\mathcal{H}}(t)\,\boldsymbol{\mathcal{H}}^\top(t)\,\mathrm{d}t\;=\;\mathbb{1}, \tag{10}$$

whereas there is coupling per individual frequency via their time derivative (with associated matrix $\boldsymbol{\mathcal{Q}}$):

$$\boldsymbol{\mathcal{Q}}=\frac{2}{T_1}\int_0^{T_1}\boldsymbol{\mathcal{H}}(t)\,\frac{\mathrm{d}\boldsymbol{\mathcal{H}}^\top}{\mathrm{d}t}\,\mathrm{d}t=\begin{bmatrix}\cdots & \cdots & \cdots & \cdots\\ \cdots & 0 & \omega_k & \cdots\\ \cdots & -\omega_k & 0 & \cdots\\ \cdots & \cdots & \cdots & \cdots\end{bmatrix}. \tag{11}$$

The ODEs (5) are weakly imposed using the same $h_j(t)$ BFs [9]:

$$\frac{2}{T_1}\int_0^{T_1}\left(\mathbf{M}\,\mathbf{X}+\mathbf{N}\,\frac{\mathrm{d}\mathbf{X}}{\mathrm{d}t}\right)h_j\,\mathrm{d}t=\frac{2}{T_1}\int_0^{T_1}\mathbf{F}\,h_j\,\mathrm{d}t, \tag{12}$$

leading to one system of $n\cdot n_\mathrm{h}$ algebraic equations:

$$\mathbf{M}^\mathrm{H}\mathbf{X}^\mathrm{H}\;=\;\mathbf{F}^\mathrm{H}, \tag{13}$$

$$\mathbf{M}^\mathrm{H}=\mathbb{1}\otimes\mathbf{M}+\boldsymbol{\mathcal{Q}}\otimes\mathbf{N}, \tag{14}$$

$$\mathbf{F}^\mathrm{H}=\frac{2}{T}\int_0^{T}\boldsymbol{\mathcal{H}}(t)\otimes\mathbf{F}(t)\,\mathrm{d}t. \tag{15}$$

IV. Homogenization of Multi-Turn Windings

A. Skin- and proximity-effect coefficients

We consider a representative FE model of the winding comprising at least one central cell (copper wire plus insulation), possibly surrounded by one or more layers of cells ($n_\mathrm{M}\geq 1$).

Frequency-domain calculations are carried out for the sinusoidal time variation at frequency f [4]. A complete characterization of the winding is achieved through the active and reactive power absorbed by the central cell and the extraction of four dimensionless frequency-dependent coefficients p_I, q_I and q_B, p_B (depicted in Fig. 1) [4]. The corresponding complex skin-effect impedance $\boldsymbol{Z}_{skin}(f)$ and complex proximity-effect reluctivity $\boldsymbol{\nu}_{prox}(f)$ read:

$$\boldsymbol{Z}_{skin}(f)=p_I(f)\;R_{DC}+\imath\;q_I(f)\;\omega\frac{\mu_0 l}{8\pi}, \tag{16}$$

$$\boldsymbol{\nu}_{prox}(f)=q_B(f)\;\nu_0+\imath\;p_B(f)\;\frac{1}{4}\lambda\sigma r^2\omega, \tag{17}$$

with ν_0 the reluctivity of the air, $r=\sqrt{\mathcal{A}_c/\pi}$ the equivalent radius (surface area $\mathcal{A}_c$), λ the fill factor and $\imath$ the imaginary unit. The DC resistance of the conductor is $R_{DC}=l/(\sigma\mathcal{A}_c)$ with l the length along the third dimension (that can arbitrarily be taken to be 1 m). It is worth mentioning that the skin-effect losses are often negligible with respect to the proximity-effect losses. Further, the skin-effect losses and the coefficient p_I are practically independent of the fill factor λ.

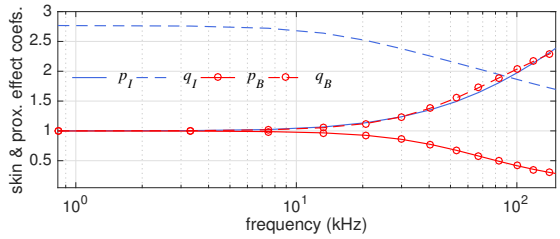

Fig. 1. Skin & proximity effect coefficients vs. frequency for round copper conductors with square packing ($\sigma=60$ MS/m, $\mathcal{A}_c=1\,\mathrm{mm}^2$, $\lambda=0.65$)

B. Homogenization in a HB-FE model

In (1) eddy currents are explicitly accounted for via $\mathbf{T}_M$ (classical FE) or via a frequency-dependent complex reluctivity (17) in the homogenized winding window (one stranded inductor) in $\mathbf{S}$ and a complex impedance (16) replacing the DC resistance in $\mathbf{R}_S$.

In the multi-harmonic case, we adopt a different proximity-effect complex reluctivity (17) and skin-effect impedance (16) per considered frequency f_k.There is a coupling between the cosine and sine HB-BFs due to these effects. The matrix $\mathbf{M}^\mathrm{H}$ is modified by considering $\boldsymbol{\nu}_{prox}(f_k)$ (17) in $\mathbf{S}$ as:

$$\begin{bmatrix}\cdots & \cdots & \cdots & \cdots\\ \cdots & \mathbf{S}(\Re(\boldsymbol{\nu}_{prox}(f_k))) & \mathbf{S}(\Im(\boldsymbol{\nu}_{prox}(f_k))) & \cdots\\ \cdots & -\mathbf{S}(\Im(\boldsymbol{\nu}_{prox}(f_k))) & \mathbf{S}(\Re(\boldsymbol{\nu}_{prox}(f_k))) & \cdots\\ \cdots & \cdots & \cdots & \cdots\end{bmatrix}, \tag{18}$$

and by considering $\boldsymbol{Z}_{prox}(f_k)$ (16) in the circuit coupling blocks via $\mathbf{R}_S$:

$$\begin{bmatrix}\cdots & \cdots & \cdots & \cdots\\ \cdots & \Re(\boldsymbol{Z}_{skin}(f_k)) & \Im(\boldsymbol{Z}_{skin}(f_k)) & \cdots\\ \cdots & -\Im(\boldsymbol{Z}_{skin}(f_k)) & \Re(\boldsymbol{Z}_{skin}(f_k)) & \cdots\\ \cdots & \cdots & \cdots & \cdots\end{bmatrix}. \tag{19}$$

V. Application Example

We consider an axisymmetric inductor with a 120-turn coil with round copper conductors ($\sigma=60$ MS/m, $1\,\mathrm{mm}^2$) and square packing ($\lambda=0.65$, see Fig. 1) [4]. The total DC resistance and inductance are $R_{DC}=0.188\,\Omega$, $L_{DC}=2.726$ mH.

The magnetic core ($\mu_r = 1000$, non-conducting $\sigma = 0$) has a central 3 mm airgap [4].

A brute-force time-domain 2-D axisymmetric FE fine model of the inductor serves as reference ($n_\mathrm{M} = 120$, $n_\mathrm{S} = 0$, $n_l = 1$) and validation of the proposed HB-FE model with homogenization. By way of illustration, flux lines obtained with a mono-frequency $f = 50\,\mathrm{kHz}$ voltage computation are depicted in Fig. 2. The eddy-current effects are clearly visible in the fine solution (left). The homogenized solution (right) follows the pattern with high fidelity though. Note the difference in mesh density.

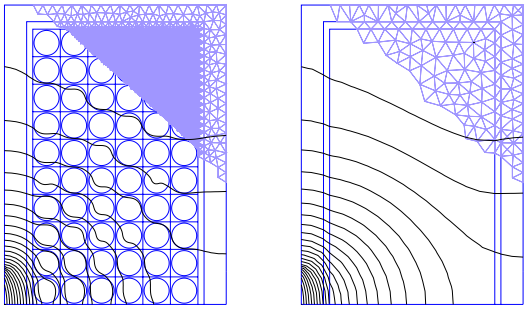

Fig. 2. Flux lines in winding domain obtained with the fine (left) and homogenized model (right). Mono-frequency domain computations with sinusoidal 50 kHz voltage. Detail of the meshes.

The equivalent resistance $R(f)$ and inductance $L(f)$ of the winding are derived from mono-frequency-domain calculations. An excellent agreement is observed in Fig. 3. Mainly due to the proximity effect, the eddy-current losses increase substantially with frequency, whereas the inductance decreases. The R and L values corresponding to the f_k frequencies considered next in the HB computation are highlighted.

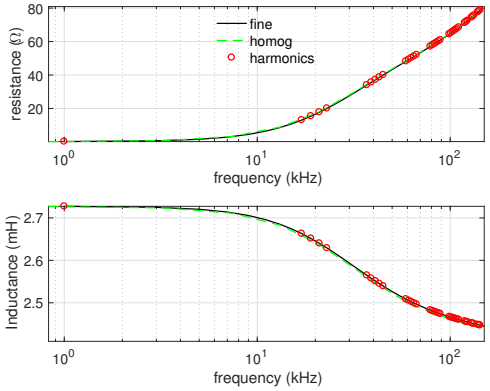

Fig. 3. Resistance (up) and inductance (down) as a function of frequency.

We consider an intersective pulse-width modulated (PWM) voltage supply (50 V DC, fundamental frequency $f_1 = 1\,\mathrm{kHz}$, modulation index $m_f = 21$, amplitude index $m_a = 0.8$, bipolar switching). The voltage waveform and main harmonic components are represented in Fig. 4. The voltage waveforms corresponding to $n_\mathrm{f} = 1, 6$, and 13 frequency harmonics are depicted as well. The frequencies included in the HB computations are chosen and sorted according to the decreasing amplitude of the PWM voltage components, e.g. the result denoted HB 6 (43) includes $n_\mathrm{f} = 6$ harmonic frequencies, harmonics 1, 21, 19, 23, 41 and 43, with the highest harmonic between parenthesis. The actual harmonics per HB case are successively added and highlighted Fig. 4 (down).

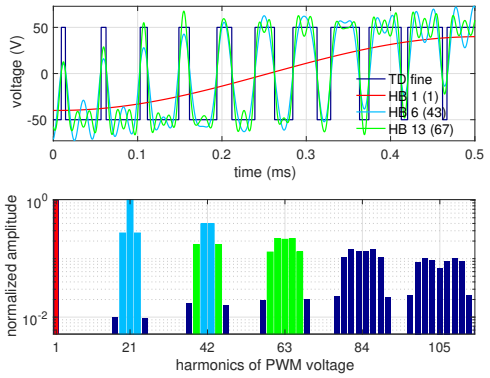

Fig. 4. Imposed PWM voltage in ref. TD-FE fine case; imposed voltage with the HB-FE model for 1 (fundamental), 6 and 13 harmonics (up). Main harmonic components of the PWM voltage (down).

Time-stepping simulations (with and without homogenization) are carried out for validating the HB approach. The pseudo time constant at $f_1 = 1\,\mathrm{kHz}$, $\tau = L/R = 11\,\mathrm{ms}$, is quite high (long transient). To prevent the lengthy transient computation, we determine an optimal phase shift for the sinusoidal control signal of the PWM voltage, with TD computations and an initial guess $\phi = \arctan(\tau f_1) = 89.9°$. A zero DC component is achieved with $\phi = 88.1°$. With this phase shift, the steady state solution is thus attained by discretising only one period with $m_f 250 = 5250$ steps.

The current computed with the homogenized winding HB approach (1, 6, 13 freqs.) is compared to the reference TD result in Fig. 5, up. The harmonic amplitudes are also depicted in Fig. 5, down. A zoom on the evolution of the current

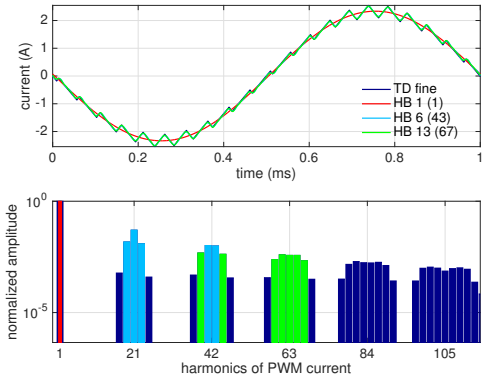

Fig. 5. Current calculated with ref. time-domain FE and homogenized winding HB-FE model and increasing harmonic components (up). Main harmonic components of the current (down).

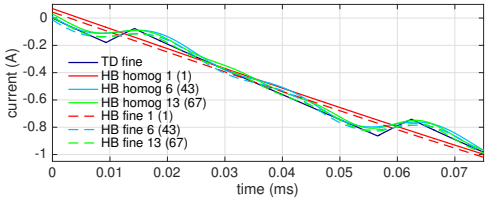

Fig. 6. Current calculated with ref. TD and HB homogenized winding FE model and increasing harmonic components (up).

with time is shown in Fig. 6. Results include the HB solution obtained with the same fine mesh as reference TD case. As expected, the accuracy of the HB approaches increases with the number of frequencies; the difference between both HB cases is evident. This discrepancy is better quantified by means of the relative L_2-error in Fig. 7, function of the number of harmonics and computed with regard to *TD fine*. For 1, 6 and 13 harmonics, the error amounts to 5.6%, 1.1%, 0.6% (*HB fine*) and to 5.7%, 1.1%, 0.8% (*HB homog*).

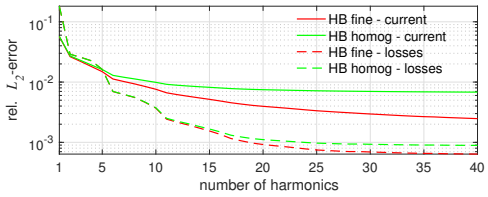

Fig. 7. Relative L_2-error on current and losses vs the number of harmonics.

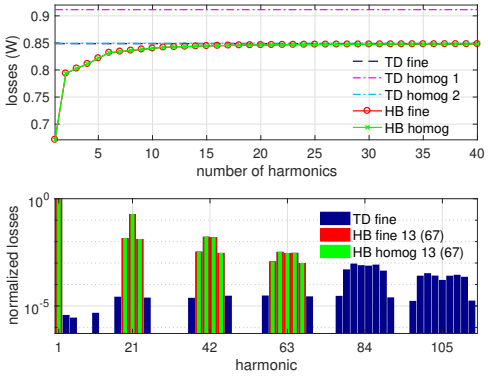

Fig. 8. Joule losses vs the number of harmonics (up). Contribution to total losses per harmonic (down).

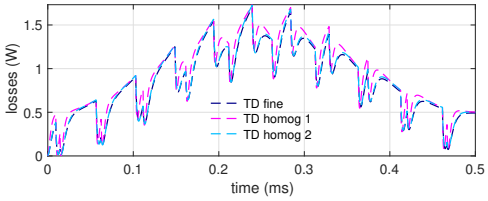

Fig. 9. Instantaneous losses obtained with TD fine and homogenized models.

For the sake of completeness, the instantaneous losses obtained with a TD homogenized approach are shown in Fig. 9. We need *TD homog* with order 2 (see [3], [4]) for ensuring a good accuracy. Regarding the current, the difference between *TD homog* order 1 and 2 is negligible and results match *TD fine* in Fig. 6.

The eddy-current losses are represented in Fig. 8 as a function of the number of harmonics (up) and as individual contribution per harmonic (down). The losses of the *TD fine* and *TD homog* 2 cases (average losses of a period in steady state) equal 0.85 W. Further, the relative L_2-errors on the HB-losses (with the *TD fine* losses as reference) are given in Fig. 7. With 1, 6 and 13 frequencies, the relative L_2-error is 18.1%, 0.7% to 0.2% (both *HB fine* and *HB homog*).

Simulations have been performed on a personal laptop with a 2.7 GHz Intel Core i7 processor and 16Gb 1600 MHz DDR3 memory. A direct LU solver is used. The cost of *TD fine* (one period, most favorable case) is: 30936 degrees of freedom (DoF), 210 Mb, 4376 s. The cost of *TD homog* 2 (one period) is: 4265 DoFs, 40.8 Mb, 249 s.

Comparing the HB approaches, we observe constant factors between the *HB fine* and *HB homog* costs (13×DoF, 19×CPU, 18×Mem). With 13 frequencies, the *HB homog* cost amounts to 92742 DoFs, 1.7 s CPU, and 0.23 Gb Mem. Even though the storage cost is higher than the one of *TD fine* and *TD homog 2* (factors 1.1 and 5.6, respectively), the gain in CPU time is considerable.

VI. Conclusions

We have embedded a homogenization method accounting for the eddy-current effects in a winding in a HB-FE method. Though validated with an axisymmetric linear case, its application is general.

An elementary and computationally cheap 2-D FE model is first used to characterize the winding type by four dimensionless frequency-dependent coefficients. The coefficients are directly used in the HB-FE model: for each of the considered frequencies in the HB approach, a different complex reluctivity and impedance value is adopted. We compare the plain time stepping with the HB approach, with and without homogenized winding. The proposed approach allows for high accuracy of local and global quantities at reduced computational cost.

Acknowledgment

Work supported by the Belgian Science Policy (IAP P7/02) and the Walloon Region under WBGreen-FEDO grant (convention n. 1217703).

References

[1] D. C. Meeker, "An improved continuum skin and proximity effect model for hexagonally packed wires," J. Comput. Appl. Math., vol. 236, no. 18, pp. 4635-4644, 2012.

[2] G. Meunier, V. Charmoille, C. Guérin, P. Labie, Y. Maréchal, "Homogenization for Periodical Electromagnetic Structure: Which Formulation?," IEEE Trans. Magn. vol. 46, no. 8, pp. 3409-3412, 2010.

[3] J. Gyselinck, R.V. Sabariego, P. Dular, "Time-domain homogenization of windings in 2-D finite element models," IEEE Trans. Magn., vol. 43, no. 4, pp. 1297-1300, 2007.

[4] J. Gyselinck, R. V. Sabariego and P. Dular, "Time-domain homogenization of windings in 3-D finite element models," IEEE Trans. Magn., vol. 44, no. 6, pp. 1302-1305, 2008.

[5] S. Yamada and K. Bessho, "Harmonic field calculation by the combination of finite element analysis and harmonic balance method," IEEE Trans. Magn., vol. 24, no. 6, pp. 2588-2590, 1988.

[6] S. Ausserhofer, O. Biro, and K. Preis, "An efficient harmonic balance method for nonlinear eddy-current problems," IEEE Trans. Magn., vol. 43, no. 4, pp. 1229-1232, 2007.

[7] H. De Gersem, S. Vandewalle, and K. Hameyer, "Krylov subspace methods for harmonic balanced finite element methods," In Lecture Notes in Computational Science and Engineering, pp. 387–396, 2001.

[8] F. Bachinger, U. Langer, and J. Schöberl, "Numerical analysis of nonlinear multiharmonic eddy current problems," Numer. Math., vol. 100, no. 4, pp. 593-616, 2005.

[9] J. Gyselinck, P. Dular, C. Geuzaine, W. Legros, "Harmonic-balance finite-element modeling of electromagnetic devices: A novel approach," IEEE Trans. Magn., vol. 38, no. 2, pp. 521-524, 2002.

[10] J. Gyselinck, L. Vandevelde, P. Dular, C. Geuzaine, W. Legros, "A general method for the frequency domain FE modeling of rotating electromagnetic devices," IEEE Trans. Magn., vol. 39, no. 3, pp. 1147-1150, 2003.

[11] H. De Gersem, K. Hameyer, T. Weiland, "Field-circuit coupled models in electromagnetic simulation," J. Comput. Appl. Math., vol. 168, no. 1-2, pp. 125-133, 2004.